Chapter 2

Experimental Procedure for the synthesis & characterization

Experimental Procedures for the synthesis and characterization

2.1 Materials Design and methods for the synthesis and characterization

This chapter deals with the method of synthesis of Bismuth Layered Aurivillius oxides and some experimental procedures carried out on these ceramic materials. In general ceramic materials are hard and brittle, shows immense stability due to their inherent quality of being heat and corrosion resistive. Their interesting properties are further enhanced by employing different compositions and synthetic routes. The purity of the synthesized materials is of utmost importance; hence single-phase formation of the materials was controlled by reaction conditions and sintering temperature. Characterization of synthesized materials to obtain information regarding microstructure and particle size were obtained using various physicochemical techniques. Few physical properties such as dielectric, impedance, magnetic and hetero-photocatalytic were investigated too at a few selected temperatures and frequencies. In the present work, following Bismuth Layered Aurivillius oxides were synthesized.

i. $Bi_4Ti_3O_{12}$-$BaTiO_3$ (BTO-BT) by modified solid-state route
ii. $Bi_4BaTi_4O_{15}$ (BBTO) by chemical route
iii. $Bi_4SrTi_4O_{15}$ (BSTO) by chemical route

The above-mentioned ceramic materials were characterized using Powder X-ray diffraction (XRD), Fourier transmission electron spectroscopy (FTIR), Transmission electron microscopy (TEM), Atomic force microscopy (AFM), Scanning electron microscopy (SEM), Energy-dispersive X-ray spectroscopy (EDX), X-ray photoelectron spectroscopy (XPS), Zetasizer Nano-ZS, UV–vis diffuse reflectance spectroscopy (DRS) UV-DRS, Brunauer-Emmett-Teller (BET). Dielectric and ferroelectric properties were detected using LCR meter at a few selected

temperatures and frequencies. Magnetic properties were observed by MPMS (SQUID magnetometer quantum design).

2.2 Material used

For the synthesis of ceramic materials, highly pure chemicals were used.

Barium nitrate, Bismuth nitrate, Strontium nitrate, Titanium oxide and citric acid with the specification are given below in table 2.1.

Table 2.1 Specification of the chemicals used.

Raw Materials	**Minimum Assay**	**Manufacturer**
$Ba(NO_3)_2$	99 %	Merck
$Bi(NO_3)_3$	99.8%	Merck
$Sr(NO_3)_2$	99.5%	Merck
TiO_2	99.8%	Merck
citric acid	99.5%	Merck

2.2 Material used

The synthesis of materials involves the following steps

Preparation of metal nitrate solution: Based on requirement of the elemental composition of the materials, elements(Ba, Bi or Sr) in the form of metal nitrates (mentioned in table 2.1) were taken as in their stoichiometric amount and dissolved in the double distilled water to form homogeneous solutions.

The $Bi_4BaTi_4O_{15}$ (BBTO) and $Bi_4SrTi_4O_{15}$ (BSTO) were successfully synthesized by chemical route whereas $Bi_4Ti_3O_{12}$-$BaTiO_3$ (BTO-BT) was synthesized by modified solid state route

This method is a type of combustion synthesis technique by use of citrate/glycine-nitrate as a complexing agent. This synthesis technique is generally useful for obtaining multicomponent single phase of the materials which is based on redox reaction between a fuel and oxidant present in the precursor solution. Generally, citric acid, glycine, urea, ethylene glycol etc., are used as a fuel and nitrates of different metals are used as an oxidant. The chelating agents like EDTA, acetic acid etc. can form a complex with metal ions present in the precursor solution and act as fuel. This complex, on dehydration, produces a viscous gel which on further heating self-ignites with the evolution of a huge amount of gases. This leads to the development of porous fluffy ash. Fine phase pure powder can be obtained on further calcinations of the ash at high temperature. In the chemical route developed, all the metal cations were taken as nitrate and Citric acid/Glycine was used as the fuel. Stoichiometric amounts of metal nitrate were dissolved in doubled distilled water and aqueous solution of citric acid per equivalent to metal ions was added to the solutions. The resulting solution was then heated on a hot plate with a magnetic stirrer at 70-80 ^{o}C to evaporate water. Dehydration of the homogeneously mixed solution during heating caused the development of a gel. This gel on further heating self-ignites followed by its swelling and obtained ignition product ash was porous in nature. The obtained precursor dry powder is calcined at a particular temperature for a certain period of time. Then, the calcined powder is ground again with the help of a mortar and pestle and converted into fine powder. An appropriate amount of polyvinyl alcohol (PVA) acts as a suitable binder is added to the powder and mixed uniformly and then it is pressed into a suitable shape.

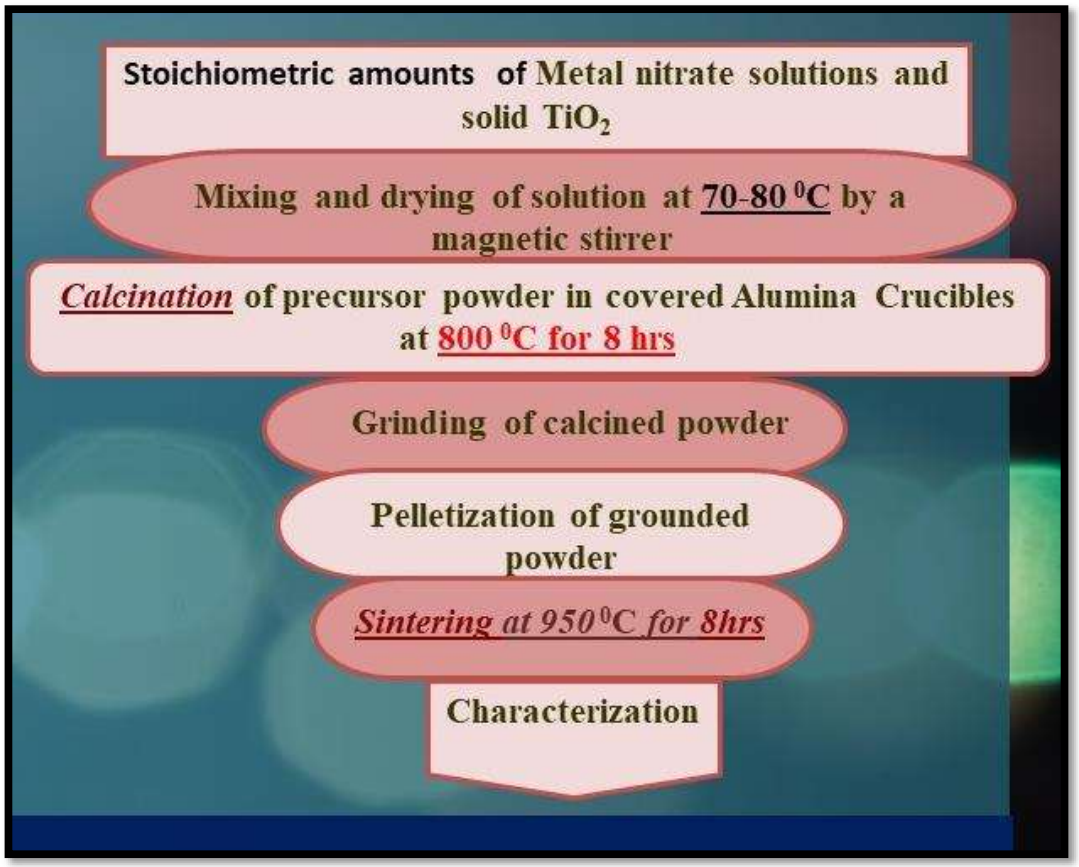

Figure 2.1 Flow chart for the synthesis of materials by chemical route.

The resulting product is first heated slowly to a particular temperature to remove the binder and then the temperature of the sample is increased to a particular value and maintained at this value for a certain duration for annealing. After annealing, the sample is cooled under controlled rate of cooling. The final resulting product is achieved by diffusion of metal ions at high temperature. A systematic flow chart of synthesis procedure is shown in figure 2.1.

2.3 Calcination Process

This process is applicable for phase transition, thermal decomposition, or removal of a volatile fraction by heat treatment from the solid powder materials. Calcination process was carried out in the absence or limited supply of air or oxygen below its

melting temperature. The synthesized materials were calcined at 800 °C for 8 hrs in a Muffle furnace (Maison et al. 2003).

2.4 Sintering Process

Sintering is the process of compacting and forming a solid mass of material, that is, densification of a porous compact by heating, without melting it to the point of liquefaction. For sintering, cylindrical pellets are required for further study of the material. For the formation of cylindrical pellets, the dry precursor of material first obtained is calcined at 800 °C for 8 h in a muffle furnace, then grinded to fine powder with the help of a pestle and mortar. To this fine calcined powder, few drops of 2%PVA were added as a binder and converted into cylindrical pellets by applying pressure of approximately 4-5 tones using a hydraulic press. The cylindrical pellets were further heated at 500 °C for 3h to evaporate the binder and then sintered at 950 °C for 8h for sintered for phase confirmation of the compounds and further used in dielectric, magnetic and ferroelectric measurements (Thiimmler and Thomma 1967).

2.5 Techniques for characterization of synthesized ceramic materials:

2.5.1 Phase and Crystal Structure Analysis:

Physical properties (electrical, magnetic, ferroelectric, optical activities etc) of any solid is decided by the three-dimensional arrangement of its constituent species (atoms, ions, molecule). Crystalline solids have unique behavior of diffracting X-ray from its characteristic planes, analysis of these diffracted X-rays gives wide variety of information about the crystals. X-ray diffraction (XRD) or High-Resolution X-ray diffraction (HR-XRD) is a proficient analytical tool that is utilized for the analysis of diffracted beam for the identification of crystalline phase and its orientation. Miller indices, Lattice parameters, crystallite size, composition of phase, are the all-other structural properties that can be determined using this technique (Smart and moore

2005; Giacovazzo et al. 2002). Every crystalline material is associated with fixed type of unit cell and position of the atoms in it, which governs the position and intensity of the X-ray diffracted peaks. Therefore, each crystalline materials have specific position and intensity of the X-ray diffracted peaks like fingerprints. Comparing data obtained from XRD with the known standards of the Joint Committee on Powder Diffraction Standards (JCPDS) file (there are more than 50,000 JCPDS cards of inorganic materials), we get the miller indices of our concerned material, which is an essential step for characterizing it.

Figure 2.2 Powder XRD instrument, RigakuMiniflex600 (Japan)

MiniFlex600 (Rigaku, Tokyo, Japan) is the XRD instrument used to record the spectra of X-ray diffraction. Main components of the instrument comprised of

generator, optics, goniometer and detector. Function of generator is to create 40 kV of tube voltage in the direction of the metal target and correspondingly a tube current of 15 mA is generated. Optical components of the instrument being the optional graphite monochromator, fixed scattering slit, and soller slit (5.0° or 2.5°). Goniometer that is employed is the vertical-type goniometer having radius 150 nm with accuracy of ±0.02°. NaI scintillator and the high-speed silicon strips are the detector that are chosen

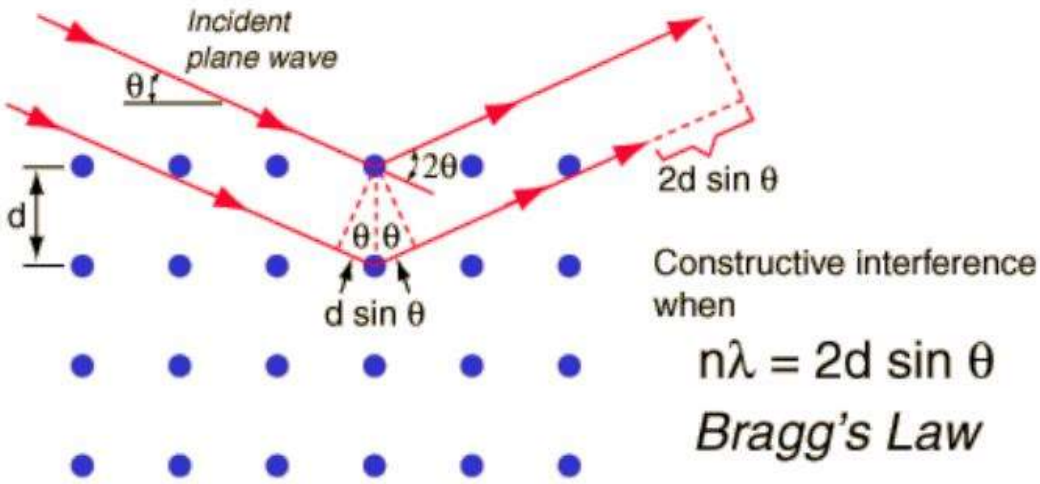

Figure 2.3 Braggs law of X-ray diffraction

The principle on which this technique is based on is the constructive interference of monochromatic X-rays radiation with crystalline materials. The X-rays employed is produced from a cathode ray tube, filtered to yield a monochromatic radiation, concentrated using collimator, which are then directed towards the sample material. The interaction of incident X-rays with the electron clouds of the atoms within the materials, results in elastic scattering of rays in all direction in the crystal (Mohammed and Abdullah). If the scattered (diffracted) rays produces a constructive interference, the relation between wavelength (λ) and inter-planar d-spacing (d) of solid powder can be expressed as Bragg's Law.

$$2d\sin\theta = n\lambda \quad (2.1)$$

Where d denotes the inter-planer spacing, λ is wavelength of incident radiation, n represents order of reflection i.e., 1, 2, 3, and θ is the Bragg angle.

The size of micrometer particles or crystallite forming the solid can be estimated by Debye-Scherrer equation as given below(Drits 1997):

$$D = \frac{k\lambda}{\beta cos\theta} \quad (2.2)$$

Here, D (in nm) represents the crystallite size; k is the dimensionless shape factor whose value is close to 0.9, λ being the wavelength of X-ray radiation, β(in radian) denotes the full width at half maximum intensity (FWHM), measuring the line broadening and θ is the Braggs diffraction angles.

2.5.2 Scanning Electron Microscopy (SEM) Analysis

Scanning Electron Microscopy (SEM) is the surface imaging method popular in modern material science research areas. SEM is a type of electron microscope in which the incident-focused electron beam of high energy scans through the sample surface and interactions with the sample generate secondary and backscattered electrons utilized to create a three-dimensional image of the sample. The image provides clear information regarding the surface topography as well as elemental compositions in the materials. The fundamental units in the instrumentation of SEM are electron-optical columns along with suitable electronics, the vacuum system including the specimen chamber, signal detection and display systems. The images obtained from signals derived from interactions of electron beam and specimen unveils information about the sample, such as external morphology (texture), elemental composition, and crystalline arrangement of materials in the specimen. Dispersion uniformity of the filler particles in the material, the size and shape of the agglomerate. To characterize the materials by the SEM instrument we need to make

them into cylindrical pellets of apt diameter and thickness, the surface of these pellets needs to be polished by using emery papers to obtain a smooth surface. However, for analysis material needs to be conducting to obtain a high-resolution good quality image, hence surface of these pellets are coated with a conducting substances such as graphite, gold, platinum, silver, chromium, osmium, gold/palladium alloy, tungsten or iridium under vacuum coating unit. Scanning Electron Microscope (SEM) (Model JEOL JSM5410) at 20 kV is the instrument that is used for the study. SEM images of the pellets of material were taken for etched polished surfaces along with the fractured surfaces. Etching on the surface of the pellet was done using HF acid for a few seconds. Average Grain size of the material was evaluated by taking root mean square of more than 100 grains diameters in image obtained by SEM with the help of Image J software of varied regions in each sample (Mohammed and Abdullah 2018).

Figure 2.4 Scanning Electron microscopy (SEM, ZEISS model, EVO18 Germany) attached with EDX Analysis instrument (Oxford instrument; USA)

2.5.3 Energy Dispersive X-ray Spectroscopy (EDX)

Energy Dispersive X-Ray Spectroscopy sometimes also called as energy dispersive X-ray analysis (EDXA) or Energy Dispersive X-Ray microanalysis (EDMXA) is a micro analytical technique that can be attached with Scanning Electron Microscopy (SEM). EDX combined with these imaging tools can give the information elemental analysis on areas as small as nanometers in diameter. The impact of the electron beam on the sample produces X-rays that are characteristic of the elements found in the sample. When the SEM electron beam bombards the sample, electrons are ejected from the atoms comprising the sample's surface. The resulting electron vacancies are filled by electrons from a higher state, and an X-ray is emitted to balance the energy difference between the two electrons' states. The X-ray energy is characteristic of the element from which it was emitted. This technique determines the elemental composition of individual points or maps out the lateral distribution of elements from selected areas such as grain and grain boundary regions of the ceramics (Scimeca et al. 2018 Mar 15). Chemical compositions and purity of the materials are investigated by EDX (Model JEOL JSM5410).

2.5.4 Transmission Electron Microscopy (TEM) Analysis

Transmission electron microscopy (TEM) is a powerful tool and extensively used technique to characterize materials. It has a distinguishing ability to form an image of atomic arrangements at a localized spot within the materials. TEM transmits a high energy beam of electrons through an ultra-thin specimen. This interaction of the electrons with the atoms in the specimen gives images used to detect features such as the crystal structure, its dislocations and the grain boundaries and shape. In comparison with light microscopes, Transmission electron microscopes use smaller de Broglie wavelength of few angstroms, providing much better resolution. This property

of the instrument facilitates it to capture even single atoms that are a thousand times smaller than an object observed by a light microscope. It is used extensively in almost every branch of science and has been useful in many applications such as virology, cancer research, material science, nanotechnology and semiconductor research (Giannuzzi and Stevie 1999). Bright-field TEM images and selected area diffraction patterns (SAED) were obtained by transmission electron microscope (TEM, FEI Tecnai-20G^2) equipped with LaB_6 filament with an accelerating voltage of 200 kV.

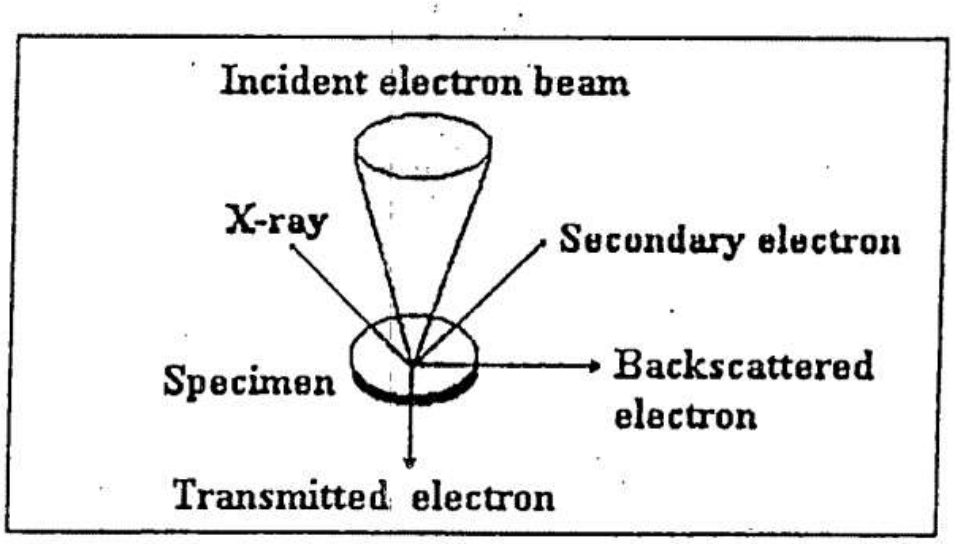

Figure 2.5 Signal produced near the surface of specimen due to interaction with electron beam.

For TEM measurement, a pinch of fine sintered powder of the concerned material was thoroughly dispersed in ethanol using an Ultrasonic Bath Sonicator. A drop of this dispersed solution was poured on a carbon-coated copper grid and kept in the oven at approximately 50 $^{\circ}$C up to 24 h to dry the sample. Then the dry sample is ready for TEM analysis. TEM micrographs depict the image of the material, confirming the nanocrystalline nature of it. The diffraction pattern was observed through the SAED pattern, and on the basis of standard bismuth layered aurivillius oxides, the HR-TEM image has been indexed .

Figure 2.6 Transmission electron microscope (TEM, FEI Tecnai-20G^2)

Atomic force microscopy (AFM) is a category of scanning probe microscopy (SPM), which signifies high-resolution of an order of fractions of nano-meters and exhibits resolution 1000 times better than the conventional optical diffraction limit. Atomic Force Microscope (Bruker, Dimension Edge with Scan Asyst) uses tapping mode on the surface of the material for measurement of average roughness and particle size distribution. AFM provides three major area of characterization: force measurement, imaging, and manipulation.

AFMs use force measurement to measure the forces operating between the sample and the probe based on their mutual separation. This becomes the basis for performing force spectroscopy, which gives data about the sample's Young's modulus, stiffness and other mechanical properties of the sample. Imaging is most used facility

provided by AFM, it employs the reaction force on the probe that is imposed by the sample to form a high-resolution three-dimensional shape image (topography) of the sample surface. This imaging is done by raster scanning the position of the sample with respect to the tip of the probe and recording the valley height of the probe that synchronizes to constant probe-sample interaction. The surface three-dimensional shape image (topography) is generally depicted as a pseudo colour plot. Manipulation in AFM provides a platform to alter the properties of the sample in a controlled manner by utilizing the tapping force of the tip on the sample surface. Atomic manipulation, local stimulation of cells and scanning probe lithography are such forms of manipulation (Hoo et al. 2008).

2.5.6 Superconducting quantum interference device (SQUID)

Magnetometry, implies to the measurement of the magnetic moment m or magnetization M of a sample. One of the highly sensitive magnetometers superconducting quantum interference device (SQUID) (Quantum Design, MPMS 3) **is** used for magnetic characterization of nanoparticles over a wide range of temperatures and used to measure extremely subtle applied magnetic fields (Bhattacharya et al. 2015; McElfresh 1994). The presence of a superconducting coil in SQUID magnetometers requires the employ of liquid helium in order to operate and to determine samples at low temperatures. Magnetic measurements were performed on a superconducting quantum interference device (SQUID) (Quantum Design, MPMS 3). Field-dependent magnetization curves in the temperature range 5-300 K at a maximum magnetic field of 5 T were performed. Measurements were also taken in both zero-field cooled (ZFC) and field cooled (FC) conditions, temperature-dependent magnetization curves were recorded from 2 to 300 K under an applied magnetic field of 200 Oe (Lyttkens et al. 1976).

Figure 2.7 Superconducting quantum interference devices (SQUID) (Quantum Design, MPMS 3)

2.5.7 Electric and Dielectric Measurement:

The prepared sintered cylindrical pellets is now ready to use for measuring the electric and dielectric properties of the material. But still few preparatory steps is required to prior to the measurement. In order to make the pellet conducting on the surface, it is first polished with emery paper to avoid roughness then coated with Ag paint on both sides, later dried over at 100 $^{\circ}$C for 30 mins. LCR Meter (PSM 1735, Newton 4th Ltd, U.K.) is now employed to measure the resistance (R), capacitance (C) and dielectric loss (tan δ) of the ceramic using cylindrical pellets. The temperature range of 300-500 K was studied in the frequency range of 100 Hz to 20 MHz with the 1 V of bias voltage. The capacitance(C), resistance (R) and dielectric loss (tan δ) of the

cylindrical pellet of the ceramic was calculated by the LCR Meter (PSM 1735, Newton 4th Ltd, U.K.) as function of temperature 300-500 K in the frequency range (100 Hz to 20 MHz) with a bias voltage of 1 Volt (Dumbrava and Svilainis 2007). Obtained capacitance and conductance data is used to calculate the dielectric constant (ε) and dielectric loss values of the materials with help of relations given in following equations :

$$C = \varepsilon_0 \varepsilon_r A / d \tag{2.3}$$

$$\varepsilon = \frac{C \times d}{\varepsilon_0 A} \tag{2.4}$$

$$\tan \delta = \frac{\varepsilon''}{\varepsilon'} \tag{2.5}$$

where, C is the capacitance (in farad), ε_0 represents dielectric constant of free space having value 8.854×10^{-12} F/m, ε indicates dielectric constant of material, A is the area (in m^2) of the electrical conductor and d is the thickness (m) of the dielectric layer (thickness of the cylindrical pellet).

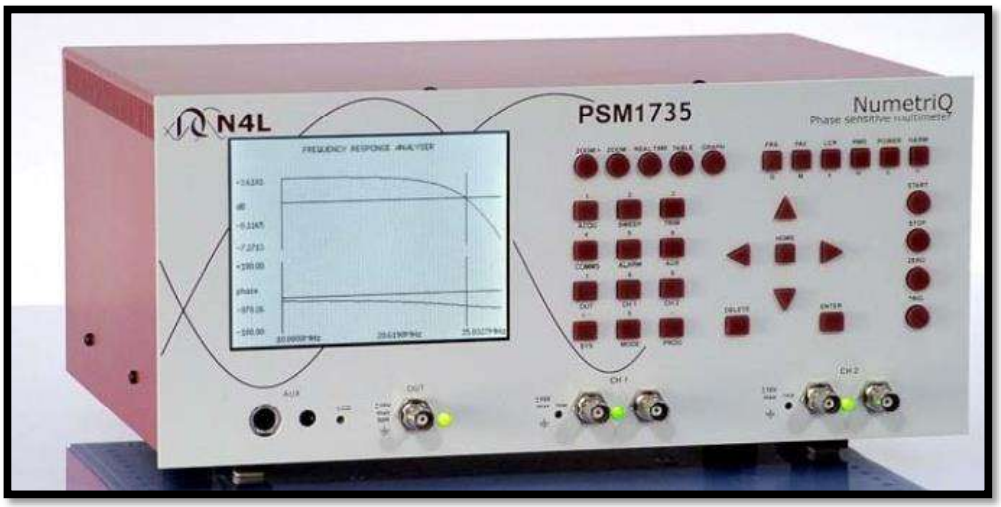

Figure 2.8 LCR Meter (PSM 1735, Newton 4th Ltd, U.K.) used for dielectric measurement

Analysis of dielectric and electrical properties was done as a function of temperature and frequency to comprehend the overall dielectric and electrical behavior of the ceramics. For estimation of the separate contributions of grains, grain boundaries and electrode polarization effect towards the values of resistance and capacitance of the material, Impedance analysis was further carried out (Kendall et al. 1996).

2.5.8 Impedance and Conductivity

The impedance spectroscopy is based on the simple resistor–capacitor (RC) equivalent circuit and the modified constant phase element (CPE) circuit, and the calculated curves agree well with the measured curves obtained in the CPE circuit. The capacitance and resistance of the grain boundaries and grains can be adjusted by altering the annealing conditions (Kumar et al. 2020). Under an anaerobic annealing atmosphere, the electric resistance values of the grain boundaries changed significantly, but the resistance of the grains exhibited almost no change. While aerobic annealing atmosphere, the phenomena got reversed. Consequently, it is established that the source of the semi conductivity of the grains in composite polycrystalline films generates from their oxygen-loss, whereas the grain boundaries are nigh to oxygen-stoichiometry (Wang et al. 1993).

2.5.9 Automatic PE loop tracer

It is a device designed for the ferroelectric characterization of materials. The output of the device gives the plots of polarization against the electric field, which is studied for ferroelectric measurement of the materials. These measurements were taken at varied frequencies ranging from 50 Hz to 1 kHz. The measurement system of the instruments comprises of a furnace with temperature controller, PE main unit along with the sample holder. PE test system based on the principle of Sawyer-Tower circuit in which two capacitors one concerned material and other the reference capacitor, are

connected in series and AC voltage applied on the series such that charges on both capacitors are the same. Another condition that must be noted that in order to obtain complete saturation, the internal capacitance must be greater than the sample capacitance (Want et al. 2016). An scheme of Sawyer-Tower circuit (Qiu et al. 2013)is shown in the figure 2.8.

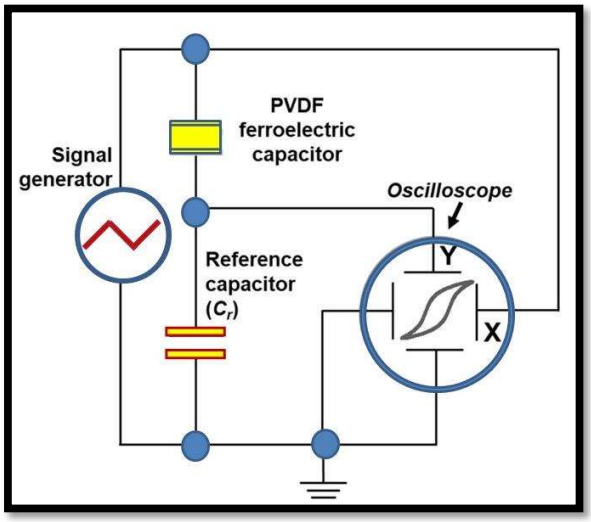

Figure 2.9 Sawyer-Tower circuit

2.5.10 Malvern Zetasizer Nano ZS

Figure 2.10 Malvern Zetasizer Nano ZS (Particle Size Analyzer)

The Malvern Zetasizer is a high-performance nano range instrument providing a platform to detect two crucial characteristics of particles of solids or molecules present in a liquid medium. These fundamental parameters are the particle size and the zeta potential. By using the non-invasive backscatter (NIBS) system optics technology operative in the Zetasizer system, the above-mentioned parameters can be measured at wide range of concentrations using dynamic light scattering (Feng and Huang 2001). Size in the range of 0.3 nm to 10 um and Zeta-potential in the broad range of 3.8nm to 100um can be estimated. The instrument has flow mode option which enables the system to be employed as a size detector of nanoparticles. Autotitration is another feature operative in The Zetasizer system, which enables it to study the consequences of changes in pH or conductivity (Allouni et al. 2009).

2.5.11 Brunauer–Emmett–Teller (BET) theory

Figure 2.11 Brunauer–Emmett–Teller (BET)

Many of the unique, intrinsic properties associated with nanomaterials arise from the large surface-to-volume ratio of these exceptionally small materials. Surface area properties may also be relatable to environmental fate and hazard implications; therefore, accurately measuring surface area is extremely important for material characterization. The most commonly used method of measuring the surface area of nanomaterials is the Brunnauer-Emmett-Teller (BET) surface adsorption method (Xiang et al. 2011).

This technique aims to explain the physical adsorption of gas molecules on a solid surface and serves as the basis for an important analysis technique for the measurement of the specific surface area of materials using the following BET equation

$$\frac{1}{v\left[1-\frac{p_0}{p}\right]} = \frac{c-1}{v_m c}\left(\frac{p}{p_0}\right) + \frac{1}{v_m c} \tag{2.6}$$

where p and p_0 are the equilibrium and the saturation pressure of adsorbates at the temperature of adsorption, respectively. v is the adsorbed gas quantity (for example, in volume units) while v_m is the monolayer adsorbed gas quantity. c is the BET constant (Rouquerol et al. 2007).

2.6 References

Allouni ZE, Cimpan MR, Høl PJ, Skodvin T, Gjerdet NR. 2009. Agglomeration and sedimentation of TiO2 nanoparticles in cell culture medium. Colloids and Surfaces B: Biointerfaces. 68(1):83–87. doi:10.1016/j.colsurfb.2008.09.014.

Bhattacharya S, Maiti R, Sen MB, Saha SK, Chakravorty D. 2015. Anomalous enhancement in the magnetoconductance of graphene/$CoFe_2O_4$ composite due to spin–orbit coupling. J Phys D: Appl Phys. 48(43):435002. doi:10.1088/0022-3727/48/43/435002.

Drits V. 1997. XRD Measurement of Mean Crystallite Thickness of Illite and Illite/Smectite: Reappraisal of the Kubler Index and the Scherrer Equation. Clays and Clay Minerals. 45(3):461–475. doi:10.1346/CCMN.1997.0450315.

Dumbrava V, Svilainis L. The Automated Complex Impedance Measurement System. :4.

Feng S, Huang G. 2001. Effects of emulsifiers on the controlled release of paclitaxel (Taxol®) from nanospheres of biodegradable polymers. Journal of Controlled Release.:17.

Giannuzzi LA, Stevie FA. 1999. A review of focused ion beam milling techniques for TEM specimen preparation. Micron. 30(3):197–204. doi:10.1016/S0968-4328(99)00005-0.

Hoo CM, Starostin N, West P, Mecartney ML. 2008. A comparison of atomic force microscopy (AFM) and dynamic light scattering (DLS) methods to characterize nanoparticle size distributions. J Nanopart Res. 10(S1):89–96. doi:10.1007/s11051-008-9435-7.

Kendall KR, Navas C, Thomas JK, zur Loye H-C. 1996. Recent Developments in Oxide Ion Conductors: Aurivillius Phases. Chem Mater. 8(3):642–649. doi:10.1021/cm9503083.

Kumar V, Kumar A, Verma MK, Singh S, Pandey S, Rai VS, Prajapati D, Das T, Singh NB, Mandal KD. 2020. Investigation of dielectric and electrochemical behavior of CaCu3−Mn Ti4O12 (x = 0, 1) ceramic synthesized through semi-wet route. Materials Chemistry and Physics. 245:122804. doi:10.1016/j.matchemphys.2020.122804.

Lyttkens J, Bergqvist I, Lodin G, Nilsson L. 1976. The ^{27}Al(d, nγ) Reaction and Bound Isobaric Analogue States in ^{28}Si. Phys Scr. 13(2):96–100. doi:10.1088/0031-8949/13/2/005.

Maison W, Kleeberg R, Heimann RB, Phanichphant S. 2003. Phase content, tetragonality, and crystallite size of nanoscaled barium titanate synthesized by the catecholate process: effect of calcination temperature. Journal of the European Ceramic Society. 23(1):127–132. doi:10.1016/S0955-2219(02)00071-7.

Mohammed A, Abdullah A. SCANNING ELECTRON MICROSCOPY (SEM): A REVIEW. :9.

Qiu X, Holländer L, Wirges W, Gerhard R, Cury Basso H. 2013. Direct hysteresis measurements on ferroelectret films by means of a modified Sawyer–Tower circuit. Journal of Applied Physics. 113(22):224106. doi:10.1063/1.4809556.

Rouquerol J, Llewellyn P, Rouquerol F. 2007. Is the bet equation applicable to microporous adsorbents? In: Studies in Surface Science and Catalysis. Vol. 160. Elsevier. p. 49–56. [accessed 2022 Jun 16]. https://linkinghub.elsevier.com/retrieve/pii/S0167299107800085.

Scimeca M, Bischetti S, Lamsira HK, Bonfiglio R, Bonanno E. 2018 Mar 15. Energy Dispersive X-ray (EDX) microanalysis: A powerful tool in biomedical research and diagnosis. Eur J Histochem. doi:10.4081/ejh.2018.2841. [accessed 2022 Jun 16]. https://www.ejh.it/index.php/ejh/article/view/2841.

Thiimmler F, Thomma W. The sintering process. METALLURGICAL REVIEWS.:40.

Wang ZL, Brynestad J, Kroeger DM, Sun YR, Thompson JR, Williams RK. 1993. Grain-boundary chemistry and weak-link behavior of polycrystalline YBa2Cu4O8. Phys Rev B. 48(13):9726–9734. doi:10.1103/PhysRevB.48.9726.

Want B, Rather M ud D, Samad R. 2016. Dielectric, ferroelectric and magnetic behavior of BaTiO3–BaFe12O19 composite. J Mater Sci: Mater Electron. 27(6):5860–5866. doi:10.1007/s10854-016-4503-8.

Xiang Q, Yu J, Jaroniec M. 2011. Enhanced photocatalytic H2-production activity of graphene-modified titania nanosheets. Nanoscale. 3(9):3670. doi:10.1039/c1nr10610d.